Fracture Mechanics of Concrete Structures, de Borst et al (eds) © 2001 Swets & Zeitlinger, Lisse, ISBN 90 2651 825 0

Drying creep: an elasto-plastic damage approach of the structural effect

F.Benboudjema, F.Meftah
LGCU - Université de Marne La Vallée, Champs sur Marne, France
J.M.Torrenti
Ecole Nationale des Ponts & Chaussées, Champs sur Marne, France

ABSTRACT: Drying shrinkage and drying creep strains represent significant components of the delayed strains occurring in concrete. Natural drying, induces not only deformation throughout the material but also a strong structural effect: the skin of the concrete dries much more quickly than the core, thereby generating tension at the skin and ultimately leading to cracking. Supported by a series of tests conducted by Granger, we will demonstrate that a model of concrete's drying and an scalar elasto-plastic damage approach enable recreating a considerable number of experimental phenomena for drying structures (loaded and unloaded). Indeed, for unloaded structures, the observed initial cracking phase and proportional shrinkage / weight loss are properly described for thick specimens. Further, the model reproduces the additional asymptotic shrinkage phase due to crack opening / closure in the case of thin specimens for which the drying is a short time process. Moreover, cracks occur at the skin of the concrete, even in the case of a compressive loading. Cracking is less pronounced in this case, but leads to an additional time-dependent deformation, namely the structural drying creep strain. Numerical simulation shows that this strain increases rapidly in the skin of the concrete, which can not bee neglected, since its value is of the same order of the elastic one. A comparison of experimental results with numerical results is made and points out that the model is able to reproduce accurately the evolution of drying shrinkage and drying creep strains.

1 INTRODUCTION

Predicting delayed strains in concrete proves to be critical to a large number of pre-stressed concrete structures, such as containment vessels of nuclear power plants. These delayed strains include:

- autogeneous shrinkage, as deformation related to the water consumption during the hydration reaction in early-age concrete: ε_{as};
- drying shrinkage, as deformation related to the moisture diffusion from the inner core to he outside of the concrete member: ε_{ds};
- basic creep strains, as time-dependent deformation of a loaded specimen, without drying: ε_{bc};
- drying creep strains, as additional deformation, which occurred in a drying and loaded specimen (Pickett effect): ε_{dc}.

Drying creep strains can not be directly separated from the other components of the delayed strains. Indeed, a drying test, a basic creep test and a total creep test need to be performed, in order to get the drying creep strains (Fig. 1). Therefore, the drying creep strains reads:

$$\varepsilon_{dc} = \varepsilon_T - \varepsilon_e - \varepsilon_{bc} - \varepsilon_{shr} \quad (1)$$

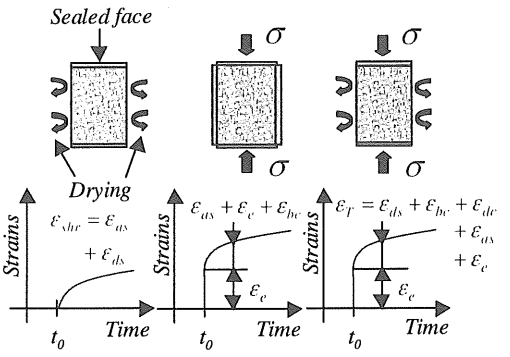

Figure 1. Experimental procedure to get the drying creep strains.

The autogeneous shrinkage strains are not considered here, since attention is given to aged specimen.

When focusing on drying shrinkage as one component of delayed strains of concrete, one can observe that this process never takes places in a homogeneous manner. It leads, in addition to deformations throughout the material, to a strong structural effect that leads to the cracking of the concrete skin (Bažant 1994). This phenomenon also partially explains the drying creep (Bažant 1994, Granger et al. 1997).

In this study, a coupled elasto-plastic-damage model (Meftah et al. 2000, Nechnech 2000) is shown to be efficient in describing experimental findings (Granger 1994) for a simple structure (cylindrical test specimen) subjected to drying and creep tests. This model allows, namely, to reproduce cracks opening-closing process with stiffness recovery. Also, irreversible strains can be simulated. These two factors are shown to be of a primary importance in reproducing the observed non-linearity in the drying shrinkage–weight loss diagram (Fig. 4). Therefore, drying shrinkage strains can be relied by a linear relationship to the weight loss, which can be identified from the linear part of the concerned diagram (Fig. 4). Furthermore, the drying process has been considered, in these simulations, as a diffusion problem governed by a parabolic-type differential equation. Solving this equation allows for computing the evolution of water content in the concrete specimen, which can be related to the drying shrinkage as explained above.

Since the drying process is properly described through the use of this appropriate damage model, the structural effect in the drying creep, when mechanical loads are concomitant to drying process, can therefore be quantified in a more accurate manner. Indeed, concrete cracking is less pronounced due to the relaxation driven by creep strains of the tensile stresses. Therefore the drying shrinkage (which was counter-balanced by skin cracking in the case of drying specimen only) appears in this case as more important. These additional induced-strains correspond, in fact, to the structural part of drying creep. It is emphasized that no basic creep model has been used. The experimental measured basic creep strain is removed from the total delayed strain in order to compare the remaining component to the simulated one.

Concerning the mechanical model, the phenomenological behavior of concrete at the macroscopic level is modeled by a coupled elasto-plastic damage approach in which the effective stress concept has been introduced (Kachanov 1986). A scalar mechanical damage variable is introduced in the relationship between the stresses and the effective stresses. This variable describes stiffness degradation concept due to mechanical cracking process. Therefore, the evolution of the mechanical damage variable is related to the physically observed crack opening represented by the plastic strain. This makes it convenient to calibrate the damage evolution from experimental results naturally based on the stress, without introducing an additional damage surface based on the strain. Furthermore, it is well known that when loading ranges between the tensile and the compressive states, the recovery of degraded stiffness is observed during unloading from the tensile region to the compressive region (Reinhardt 1984). The stiffness recovery is a consequence of the closing of the previously opened cracks. The damage variable is then splitted in two parts, one for tensile loading and the other for compressive one. This provides the separate evolution of the directional damage and then allows capturing stiffness recovery. In these simulations, the compressive behavior of concrete is considered as elastic since compressive stresses remain within the elastic domain.

2 EXPERIMENTAL RESULTS

We will be making use of the results obtained by Granger (1994), which include measurements of both weight loss and drying shrinkage on various concrete mixtures used in France in the construction of nuclear power plants. Since the shape of the curves describing these different samples is identical, only one concrete mix design will be considered for the remainder of this study (see Table 1).

Table 1. Composition of the concrete mixture (per°m^3) for the Civaux B11 specimen.

Gravel	Sand	Adjuvant	Cement	Water
1100 kg	772 kg	1.22 kg	350 kg	195 kg

The measured mechanical properties of the specimen are given in Table 2 for a 28 days old specimen:

Table 2. Mechanical properties for the Civaux B11 specimen.

Young Modulus	Poisson ratio	Strength	
		Tensile	compressive
33.7 GPa	0.248	3.7 MPa	40.2 MPa

During drying tests, the specimens are stored in a test room, where the temperature is 20°C ± 1°C and the relative humidity is 50 % ± 5 %. Figure 2 shows the experimental evolution of weight loss as a function of the square root of time. Weight loss is measured on a test specimen of 16 cm in diameter and 32 cm in height, both ends of which have been protected from drying (thus causing radial drying only). Drying shrinkage is measured on a test specimen 16 cm in diameter and 100 cm in height. Total shrinkage is measured on a 50-cm base located in the central part of the specimen, which allows avoiding all boundary effects (Fig. 3). An identically-sized

specimen protected from desiccation serves to measure the level of autogeneous shrinkage, which is then subtracted from total shrinkage in order to derive the actual drying shrinkage.

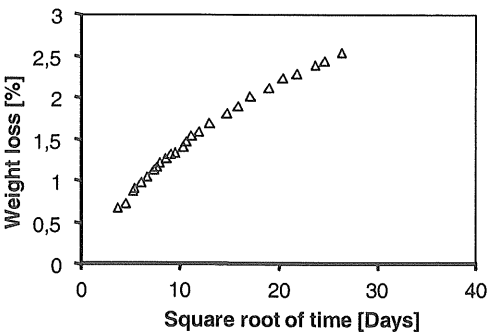

Figure 2: Weight loss as a function of square root time.

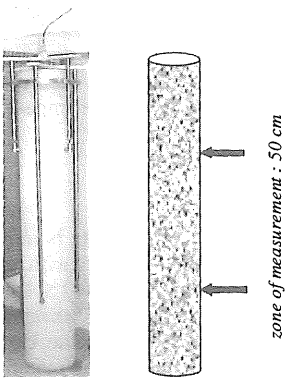

a) test : (by courtesy of LCPC, Paris, France)

b) principle : shrinkage is measured in the central part of the sample

Figure 3. Weight loss as a function of square root time.

The evolution of the drying shrinkage as a function of the weight loss shows for the considered concrete mixture together with other one (Fig. 4) the existence of three phases (Granger 1994, Bažant 1986):

- during the first phase, the water content gradient created by the drying generates a stress gradient, coupled with very high tension in the skin layer and (as a mechanical effect) cracking in the skin, yet without any shrinkage (sleeping zone);
- during the second phase, these gradients become more pronounced, the cracking in the skin remains unchanged, and shrinkage is proportional to drying (linear zone);
- during the third and final phase, the gradients disappear and the cracks would be expected to close yet this phenomenon is not entirely reversible, a condition which results in asymptotic shrinkage (non linear zone).

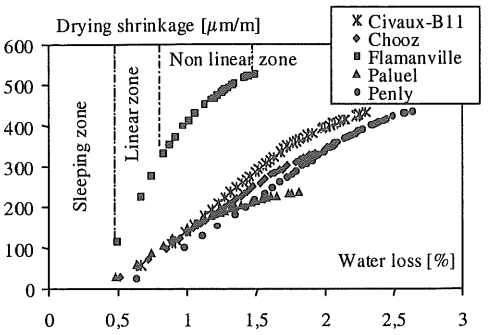

Figure 4. Drying shrinkage as a function of weight loss.

The same observations have been made recently by Bissonette et al. (1999).

These hypotheses have been confirmed by means of different models, such as the probabilistic model (Granger 1994) or with the used elasto-plastic damage approach (Meftah et al. 2000). These models allow an accurate simulation of the drying shrinkage including the cracking of the skin of the samples.

Using the same elasto-plastic damage model, we can simulate the effect of drying during a creep test. Due to the external loading, the behavior of concrete is similar to the behavior of a concrete in which the tensile strength is increased by the loading. We have fewer cracks and more strains. These supplementary strains are the structural part of the drying creep.

For the same specimen, the author (Granger 1994) also measured basic creep strains and total creep strains (Fig. 5). The applied uniaxial stress is 10 MPa. During the total creep test, the specimen is stored in the same ambient conditions that the drying shrinkage test specimen.

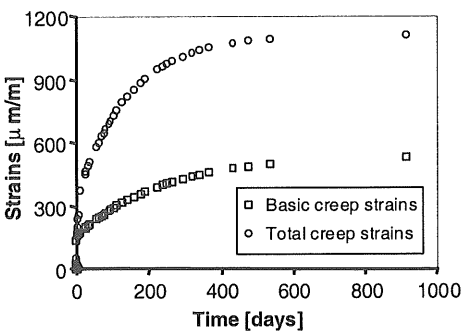

Figure 5. Basic ant total creep strains for the Civaux B11 specimen.

3 MODELING APPROACH

3.1 *Drying model*

Drying is modeled according to a very classical approach, by relying on a diffusion equation:

$$\frac{\partial C}{\partial t} = div(D(C)\cdot gradC) \qquad (2)$$

in which C is the water content and D is the diffusivity which varies in a strongly non-linear manner as a function of the water content. The diffusivity is calculated with the relation derived by Xi et al. (1994) and given by Eq.2a. However, the authors tied the diffusivity to relative humidity h instead of water content. As such, we were able to obtain the desired relationship by means of a desorption curve $h(C)$. Granger showed that a parabolic approximation of the desorption curve (Eq. 4) is sufficient to reproduce properly the experimental curve available in the literature for a similar concrete (Pihlajavaara 1982). The $D(C)$ and $h(C)$ relationships used in the computations are the following:

$$D(h) = A\cdot\left(\alpha+\beta\cdot\left(1-2^{-10^{\gamma(h-1)}}\right)\right) \qquad (3)$$

with $A = 7\times10^{-10}$, $\alpha = 0.002$, $\beta = 0.45$ and $\gamma = 4$.

$$h(C) = 1-0.5\cdot\left(\frac{C-C_0}{C_0-C_{eq}}\right)^2 \qquad (4)$$

On the basis of the concrete's composition, Granger determined the initial water content C_0 = 132.7 l/m^3. As regards the limit conditions, we have set the value of surface water content C_{eq} = 62.1 l/m^3 to correspond with the relative humidity of test specimen storage conditions (50%).

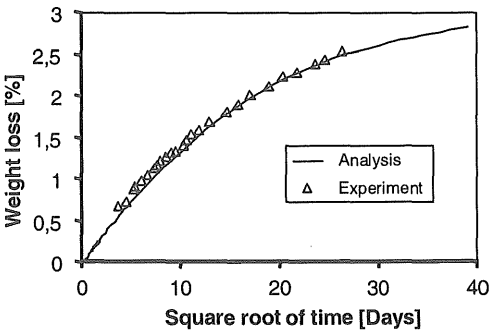

Figure 6. Comparison of measured changes in weight loss vs. computed changes.

These equations and data were then entered into the CASTEM2000 code developed by the French atomic energy commission (CEA). Figure 6 displays the comparison between computational results and experimental measurements in term of evolution of weight loss with respect to time.
From figure 6, we observe that the numerical result correlates quite well with the experimental data for the weight loss.

3.2 *drying shrinkage constitutive law*

The relation between drying and shrinkage is often based on a linear relation between drying shrinkage and the relative humidity (Wittmann 1982, Alvaredo 1994). Indeed, the desorption isotherm is almost linear if the relative humidity is higher than 50%. Therefore, in a previous study (Torrenti et al. 1999) based on the concepts forwarded by Granger (Granger 1994), the local shrinkage strain tensor ε_{ds} was been considered as proportional to the water content variation:

$$\dot{\varepsilon}_{ds} = k\cdot\dot{C}\,\mathbf{I} \qquad (5)$$

where k is held fixed on the linear section of the experimental curve at a value of $k = 1.22\times10^{-5}$, and $\mathbf{I}$ is the unit tensor. The dot represents derivation with respect to time. The computation is then carried out by taking the local shrinkage as the imposed deformation.

3.3 *Mechanical model*

The mechanical behavior of concrete is modeled by an isotropic damage model coupled with plasticity. A single scalar damage variable $0 \le D \le 1$ is used to represents the effect of progressive cracking, due to external mechanical loads. It gives the degradation of the current stiffness tensor $\mathbf{E}$ of the material:

$$\mathbf{E} = (1-D)\,\mathbf{E}_0 \qquad (6)$$

where $\mathbf{E}_0$ is the initial elastic stiffness tensor.
Since the behavior of the undamaged part of the material is elastic, the stress-strain relationship reads:

$$\sigma = (1-D)\cdot\tilde{\sigma} = (1-D)\,\mathbf{E}_0\cdot\varepsilon_e \qquad (7)$$

and the elastic strain ε_e is obtained by:

$$\varepsilon_e = \varepsilon - \varepsilon_p - \varepsilon_{ds} \qquad (8)$$

where ε is the total strain and ε_p is the irreversible strain (due to cracking).
Since numerical simulations (§ 4) show that the compressive stresses are beyond the elastic strength of the material, we will only present the features of the mechanical model in tension. For more details on the mechanical model, the reader is reported to (Nechnech 2000).
The modeling of the crack opening/closing behavior can be implemented by elastic-stiffness recovery during the elastic unloading process from tensile

state to compressive state. Thus, the tensile damage variable is modified by a scalar weight factor:

$$D = 1 - (1 - p(\tilde{\sigma})D_t) \text{ and } p(\tilde{\sigma}) = \sum_{i=1}^{i=3} \langle \tilde{\sigma}_i^p \rangle \Big/ \sum_{i=1}^{i=3} |\tilde{\sigma}_i^p| \quad (9)$$

where σ_i^p is the i^{th} component of the principal effective stress tensor σ, and $\langle x \rangle = (|x|+x)/2$ is the Macaulay's bracket function. This parameter allows to shift progressively the effect of the tensile part of damage and to get a virgin compressive stiffness, when stress state swishes from tension to compression as one can easily see in the uniaxial case. The subscript t refers to tension.

The evolution of the damage evolution is considered as of an exponential form:

$$D_t = 1 - exp(-c_t \kappa_t) \quad (10)$$

where κ_t is the tensile cumulated plastic strain and c_x a material parameter identified from experimental stress-strain curve (Nechnech 2000).

Once micro-cracks are initiated, local stresses are redistributed to undamaged material micro-bonds over the effective area. Thus, effective stresses in undamaged material points are higher than nominal stresses. Accordingly, it appears reasonable to state that the plastic flow occurs in the undamaged material micro-bounds by means of effective quantities (Ju 1989). A Rankine criterion (Fig. 7) is used in tension (Feenstra 1993):

$$F_t(\tilde{\sigma}, \kappa_t) = \tilde{\sigma}_I - \tilde{\tau}_t(\kappa_t) \quad (11)$$

where τ_t is the nominal strength in tension and σ_I is the maximal principal stress in tension. The ˜ symbol corresponds to effective quantities.

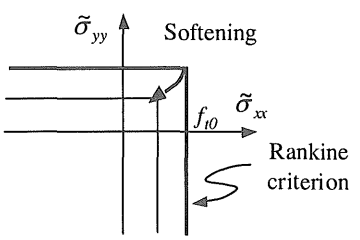

Figure 7. Loading surface defined in the principal stress plane space

The nominal strength is written as:

$$\tau_t = f_{t0}\left[(1 + a_t)\exp(-b_t \cdot \kappa_t) - a_t \exp(-2b_t \cdot \kappa_t)\right] \quad (12)$$

where f_{t0} is the initial tensile strength of the material, a_t and b_t are material parameters identified from uniaxial test (Nechnech 2000).

The plastic strain rate is then obtained by the normality rule:

$$\dot{\varepsilon}^p = \dot{\lambda}_t \frac{\partial F_t}{\partial \tilde{\sigma}} \quad (13)$$

where λ_t is the plastic multiplier.

Strain softening induces inherent mesh dependency and produces failure without energy dissipation (Pijaudier-Cabot et al. 1987). In order to avoid these shortcomings, a characteristic length is introduced. This length is related to the mesh size (Rots 1988) in order to dissipate the same energy after mesh refinement, when strains localized (as a macro-crack representation) in one row of finite elements.

In these simulations, the results of the elasto-plastic damage model are compared with the results of the Mazars's elastic damage model (Mazars 1984). The most important differences between theses two models are that the Mazars's elastic damage model doesn't take into account:

- the inelastic strain which occurs, when the material is cracked and unloaded;
- the crack-closure effect when the material is subjected to alternated loads;

4 NUMERICAL SIMULATION

The drying problem necessitates a rather thin mesh at the skin layer in order to capture accurately the drying front and reproduce correctly the shape of the water content curve. Under these conditions, the mechanical computation, for which the zones of large damage have already been located, provides sufficient accuracy.

The model parameters have been held fixed in order to reproduce the mechanical properties measured by Granger (see Table 2). Note that the experimental softening behavior of the considered concrete is not known and damage evolution can not be determined according to test results. Therefore two cases are considered, corresponding to usual value of stiffness degradation with cracking (Fig. 8).

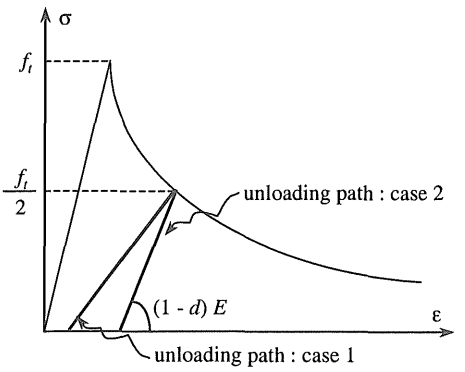

Figure 8. Two different unloading paths considering in the numerical simulations.

The first results concern the drying shrinkage test specimen. Figure 9 shows the evolution of stresses as a function of the radius at different stages. In contrary to the Mazars's elastic damage model (Torrenti et al. 2000), the plastic-damage model takes into account the closure of cracks, leading to important values of residual stresses. Indeed, even if the specimen has completely dried, differential stress distribution remains, which in plus gives rise to tensile stresses in the core of the specimen inverting, thus, the previous ones.

The peak stress indicates a progression in crack depth, which reaches 2 cm after 50 days and then remains relatively stable beyond that point. This aspect can also be shown through the profile of the damage evolution during time, all over the radius of the specimen (Fig. 10).

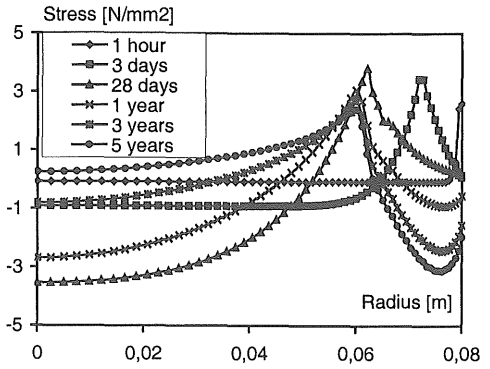

Figure 9. Stresses at different times for the drying shrinkage test specimen.

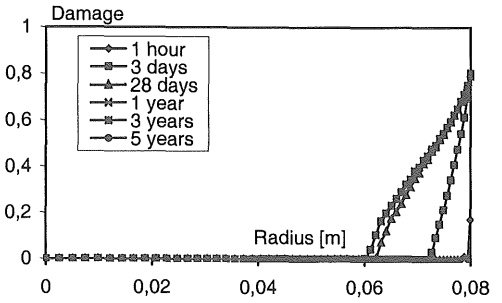

Figure 10. Evolution of damage over the radius at different times in the drying unloaded specimen.

A comparison of the evolution in shrinkage simulated by two damage models versus experimental results is plotted in Figure 11. The first model is the Mazars elastic damage model in which no inelastic strains are taken into account. The second one is the model presented above, in which crack opening is given by the plastic strain, such that compressive stresses do rise to fully close the cracks when unloading occurs in tension. Figure 11 displays very good agreement between the experimental findings and the results of both of the two models, except over the final phase for the elastic damage model. The agreement in this phase with the elasto-plastic damage model is quite well, namely in term of asymptotic behavior of shrinkage strain evolution. This outcome serves to validate the hypotheses forwarded by the authors cited above (Bažant 1986, Granger et al. 1997) regarding the structural behavior of concrete during its desiccation and the hypothesis regarding the proportionality existing between local shrinkage and local water content. These findings also demonstrate that the damage model can accurately simulate a significant portion of the drying shrinkage. Depending on the size of the test specimen, the crack-closing phase will not be attained within the structure's service life, in which case an elastic damage model proves to be a sufficient basis for modeling shrinkage. Otherwise, a full elastoplastic damage model should be used. From the figure 11, we observe also that the drying shrinkage in the case of the first unloading path (Fig. 8) is bound by second unloading path case and by the Mazars elastic damage case. It highlights the fact that inelastic strains play a major role, as the drying process ceases in the specimen, in the evolution of the drying shrinkage strains.

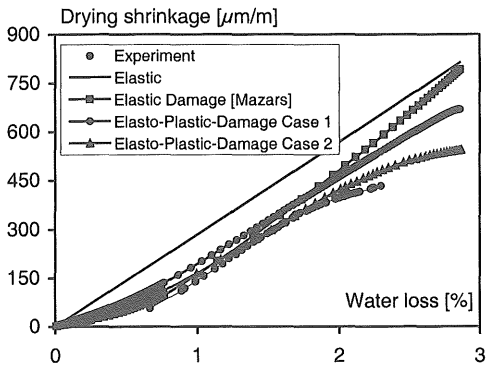

Figure 11. Comparison of experimental shrinkage curves with simulated ones by means of the Mazars's elastic-damage (Torrenti et al. 1999) and the elasto-plastic damage models.

Next, we carry out simulation on the total creep test specimen. The uniaxial applied stress is 10 MPa. Figure 12 displays the stresses profile over the radius for different stages. As in the case of the drying shrinkage test, cracks appear at the skin of the specimen due to tensile stresses, even if a compressive loading is applied. However, the depth of the cracking zone reduces significantly, as shown by

figure 13. Furthermore, the stress profile tends to the initially applied one without significant additional residual stresses.

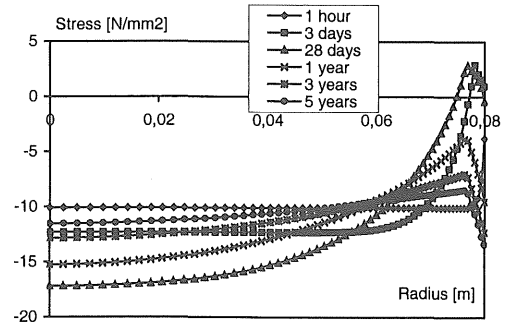

Figure 12. Stresses at different times for the total creep test specimen.

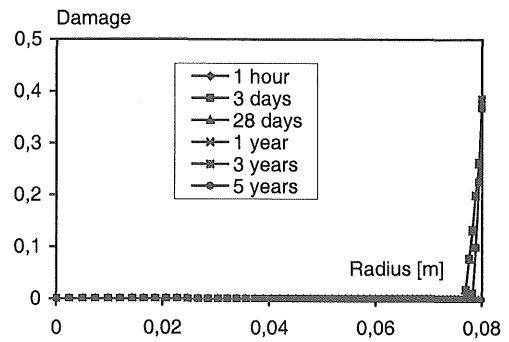

Figure 13. Evolution of damage over the radius at different times in the drying loaded specimen.

In order to compare the numerically simulated and the experimentally obtained drying creep strains, we

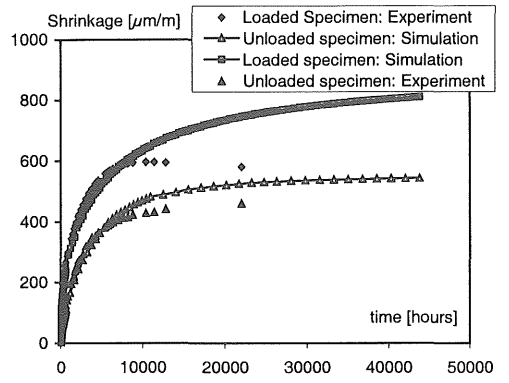

Figure 14. Evolution of drying shrinkage for both of loaded and unloaded specimen.

first plot in figure 14 drying strains for both of unloaded and loaded specimen. Since basic creep has not been considered here in the numerical simulation, experimental drying strains for the loaded specimen are obtained by removing basic creep strains from the total measured ones, in order to compare homogenous quantities.

The figure 14 shows that for the two cases a good agreement between numerical and experimental findings is achieved. However, for the loaded specimen, a scattering is observed after a certain stage of the experimental test. It corresponds to a decrease in the experimental drying strains (for the loaded specimen) when removing the basic creep component from the total measured strains as explained previously.

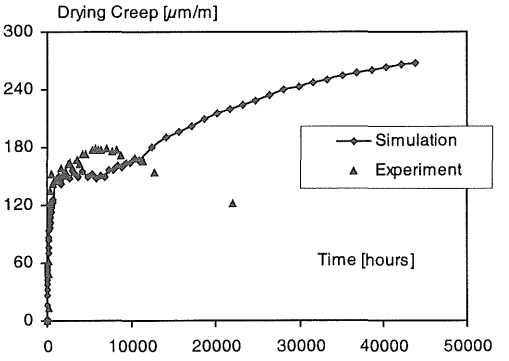

Figure 15. Comparison of test results with numerical results for the drying creep strains evolution with respect to time.

Drying creep strains can now be obtained by removing the drying strains measured on the unloaded specimen from the drying strains of the loaded on. Figure 15 displays the comparison of the numerical results and the experimental counterparts. It can be observed that the gap between the two curves is more pronounced due, again, to a significant decrease in the experimental drying creep strains. However, the agreement between experiment and simulation remains acceptable particularly at early stages. This means that even an elastic damage model can predict this early part of the experiment since the irreversible strains and cracking closure process do not act significantly yet. Nevertheless, inherent errors related to measured values can also be incriminated, namely when removing the basic creep strains by considering them no influenced by the moisture change within the specimen.

At last, figure 15 indicates that drying creep strains increase rapidly in the skin of the specimen, during the first days. Drying creep can not be neglected in the case of a structure calculus, since its value is of the same order of the elastic one (about 300 μm/m).

5 CONCLUSION

Through the use of a damage model, coupled with a classical water diffusion model and by assuming that local shrinkage is proportional to local water content, we have confirmed a number of hypotheses forwarded by various authors, namely:

- the drying of concrete begins by a phase of skin cracking which does not give rise to drying shrinkage;
- afterwards, drying shrinkage becomes proportional to weight loss.

An elastic damage model proves to be adequate for thick test specimens in that the phase corresponding to the crack closure (as the drying process ceases) will never be reached within the structure's service life (such tends to be the case with containment shells at nuclear power plants). In order to simulate accurately this final phase for relatively-thin specimens as well, it is however necessary for the model to take into account the occurrence of inelastic strains as skin tension stresses decrease, which is the case on an elasto-plastic damage model. The mechanical model used in these simulations correlates well with experimental data for the drying shrinkage.

In the case of the drying and loaded specimen, cracking is less pronounced. Thus, it leads to additional strains, which are the structural part of the drying creep. Numerical simulations show that the elasto-plastic damage model fits pretty much with experimental drying strains. However, a discrepancy is observed for the loaded specimen, as the experimental drying strains decrease. It may be related to the manner we obtain drying creep strains from the experimental data, since we made the assumption that basic creep strains do not depend upon the moisture change within the specimen.

In these simulations, basic creep and intrinsic drying creep strains have not been modeled. Indeed, concrete cracking is less pronounced due to the relaxation of the tensile stresses driven by creep strains. Thus, apparent drying shrinkage is underestimate. Numerical simulations have to be performed to quantify the role of creep strains.

REFERENCES

Alvaredo, A.M. 1994. *Drying shrinkage and crack formation.* Aedificatio publishers: IRB Verlag.

Bažant, Z.P. 1986. Creep and shrinkage of concrete: mathematical modeling. *Fourth RILEM symposium*, Evanston.

Bažant, Z.P. 1994. Drying creep of concrete: constitutive model and new experiments separating its mechanisms. *Materials and Structures* 27: 3-14.

Bissonette, B. & Pierre, P. & Pigeon, M. 1999. Influence of key parameters on drying shrinkage of cementitious materials. *Cement and concrete research* 29: 1655-1662.

Granger, L. 1994. Comportement différé du béton dans les enceintes de centrales nucléaires: analyse et modélisation. *ENPC thesis*, Paris (in French).

Granger, L. & Torrenti, J.M. & Acker P. 1997. Thoughts about drying shrinkage: experimental results and quantification of structure drying creep. *Materials and Structures* 30(204): 588-598.

Ju, J.W. 1989. On Energy-Based Coupled Elastoplastic Damage Theories: Constitutive Modeling and Computational Aspects. *International Journal of Solids and Structures* 25(7): 803-833.

Kachanov, L. M. 1986. *Introduction to continum damage mechanics.* Dordrecht, The Netherlands.Martinus: Nijhoff Publishers.

Mazars, J. 1984. Application de la mécanique d'endommagement au comportement non linéaireet à la rupture du béton de structure. *Thèse de doctorat d'Etat*, Université Paris VI (in French).

Meftah, F. & Torrenti, J.M. & Nechnech, W. & Benboudjema, F. & de Sa, C . 2000. An elasto-plastic damage approach for the modeling of concrete submited to the mechanical induced effects of drying. *Shrinkage 2000 Workshop*, Paris.

Nechnech, W. 2000. Contribution à l'étude numérique du comportement du béton et des structures en béton armé soumises à des sollicitations thermiques et mécaniques couplées : Une approche thermo-élasto-plastique endommageable. *Thèse de doctorat de l'INSA de Lyon*: 207

Pihlajavaara, S.E. 1982. Estimation of drying of concrete at different relative humidities and temperature of ambiant air with special discussion about fundamental features of drying and shrinkage. in *Creep and Shrinkage in Concrete Structures*, edited by Z. P. Bažant and F.H. Wittmann. New-York: John Wiley & sons.

Pijaudier-Cabot, G. & Bažant, Z.P. 1987. Nonlocal damage theory. J. of Engrg. Mech. ASCE 113: 1512-1533.

Reinhardt, H.W. 1984. Fracture mechanics of an elastic softening material like concrete. *Heron* 29(2): 1-42.

Rots, J.G. 1988. Computational modeling of concrete fracture. PhD Dissertation, Netherlands: Delft University of Technology.

Torrenti, J. M. & Granger, L. & Diruy, M. & Genin P. 1999. Modeling concrete shrinkage under variable ambient conditions. *ACI Materials Journal* 96(1): 35-39.

Torrenti, J.M. & de Sa, C. 2000. Finite element modeling of drying shrinkage. *ASCE Proc. Eng. Mechanics*, Austin.

Wittmann, F. 1982. Creep and shrinkage mechanisms. in *Creep and shrinkage in concrete structures*, edited by Z.P. Bažant and F.H. Wittmann, New-York: John Wiley & sons.

Xi, Y. & Bažant, Z.P. & Jennings, H. & M. 1994. Moisture diffusion in cementitious materials - adsorption isotherms. *Advanced Cement Based Materials* 1: 258-266.